Journal of Solid State Chemistry **155,** 458–462 (2000)
doi:10.1006/jssc.2000.8995, available online at http://www.idealibrary.com on IDEAL®

RAPID COMMUNICATION

Magnetic Iron Oxide/Mullite Nanocomposite Stable up to 1400°C

M. P. Morales,* T. González-Carreño,* M. Ocaña,† M. Alonso-Sañudo,* and C. J. Serna*

*Instituto de Ciencia de Materiales de Madrid, CSIC, 28049 Cantoblanco, Madrid, Spain; and †Instituto de Ciencia de Materiales de Sevilla, CSIC, Avda Americo Vespucio s/n, 41092 Sevilla, Spain

Received June 2, 2000; in revised form September 20, 2000; accepted October 6, 2000; published online November 29, 2000

Magnetic nanocomposites consisting of spherical iron oxide particles of around 13 nm dispersed in a mullite matrix have been obtained by pyrolysis at 600°C of an aerosol generated from a solution of TEOS and iron and aluminum nitrate in methanol and a posterior heat treatment at 1200°–1400°C. Iron contents higher than the solubility limit of Fe in mullite (12 wt% Fe_2O_3) have been used to prepare the precursor samples. It should be emphasized that the new magnetic nanocomposite presents a saturation magnetization of 3.3 emu/g and a coercivity of 546 Oe at room temperature, and preserves its magnetic character up to 1400°C. This behavior reveals that mullite is an excellent matrix to keep the magnetic particles apart, avoiding sintering during the heat treatment and therefore making phase transformations difficult. © 2000 Academic Press

Key Words: **spray pyrolysis; magnetic nanocomposite; iron oxide nanoparticles; magnetic properties.**

INTRODUCTION

Nanocomposite materials containing magnetic particles are very interesting in many applications since they exhibit new exciting electronic, magnetic, and optical properties (1–3). These composites have been produced in a variety of matrix materials such as silicon oxides (4–6), aluminum oxides (7), porous glass (8), vesicles (9), and polymers (10). The pore structure of the matrix and the interactions between magnetic particles and host seem to control, at least in part, the magnetic properties and stability of the composite. The excellent thermal stability is an intrinsic advantage of the inorganic nanocomposites in contrast to the low thermal stability and the high elasticity of the polymeric matrices (11). However, the thermal stability range is limited for some inorganic matrices, such as SiO_2 and Al_2O_3, since they interact with the particles at temperatures higher than 600°C (6). Also, at this temperature, the diffusion inside the matrix is favored, which may induce aggregation of the magnetic particles and possible phase transformations. This has been observed, for example, in the case of γ-Fe_2O_3 particles encapsulated in a silica–zirconia matrix, which transformed into α-Fe_2O_3 on calcination at 900°C (12) due to the increase in particle size, which makes the γ–α transformation easier (13).

The mullite structure is suitable for the incorporation of foreign cations such as iron, which preferably substitutes for Al at octahedral lattice sites (14, 15). It has been shown that when the solubility of Fe in mullite is overtaken, additional iron oxide phases consisting of an iron oxide spinel can be formed (15, 16). Therefore, it would be interesting to study the composition range for the formation of such composites and its magnetic properties. With this purpose, iron oxide/mullite composites have been prepared by pyrolysis of aerosols generated from solutions of TEOS and Fe and Al nitrate in methanol. Fe contents above the solubility limit of Fe(III) in mullite ($\sim$ 12% Fe_2O_3) and temperatures higher than 1000°C have been used in order to promote the crystallization of mullite. Sample characterization was carried out by X-ray diffraction, thermogravimetric analysis, and transmission electron microscopy. Magnetic behavior of the composites was studied from the hysteresis loops at room temperature. It should be emphasized that the composites reported here show unusual magnetic properties after heating at very high temperature (1400°C).

EXPERIMENTAL

Iron oxide/mullite nanocomposites were obtained by heating at temperatures higher than 1000°C the Fe-doped silica–alumina powders prepared by pyrolysis of an aerosol following the method described elsewhere (15). A methanol solution containing tetraethylorthosilicate (TEOS), Al $(NO_3)_3.9H_2O$, and $Fe(NO_3)_3.9H_2O$ was sprayed through a furnace heated at 250°C where the solvent is evaporated and afterward through a second furnace at 600°C where the metal precursors are decomposed. The resulting amorphous powder was finally collected in an electrostatic precipitator

0022-4596/00 $35.00
Copyright © 2000 by Academic Press
All rights of reproduction in any form reserved.

TABLE 1
Initial Solution Concentration for the Preparation of the Al-Doped Mullite Samples

Sample	Initial solution concentration (M)			Nominal composition
	TEOS	$Al(NO_3)_3.9H_2O$	$Fe(NO_3)_3.9H_2O$	
M10	0.025	0.0625	0.0125	$Fe_1Al_5Si_2O_{13}$
M20	0.025	0.05	0.025	$Fe_2Al_4Si_2O_{13}$
M30	0.025	0.0375	0.0375	$Fe_3Al_3Si_2O_{13}$

and later heat-treated at 1200 and 1400°C for 4 h to promote the formation of iron oxide/mullite composites. The TEOS concentration in the initial solution was kept constant and equal to 0.025 M while the aluminium and iron concentration were varied (Al + Fe = 0.075 M) in order to get the final compositions: $Fe_1Al_5Si_2O_{13}$, $Fe_2Al_4Si_2O_{13}$, and $Fe_3Al_3Si_2O_{13}$ (samples M10, M20, and M30, respectively) as shown in Table 1.

The nature of the heated samples was examined by X-ray diffraction in a Philips PW 1714 diffractometer, using Cu$K\alpha$ radiation and a graphite monochromator. Diffractograms were recorded between 5° and 70° (2θ) at 0.04° 2θ/s. The evolution with temperature of the powders collected after pyrolysis was followed by thermal analysis (TG and DTA). The measurements were carried out in a Staton Redcroft Thermal analyzer STA-780 apparatus in air at a heating rate of 10°C min^{-1}. Estimation of the particle size and shape and the degree of dispersion of the magnetic particles inside the mullite matrix were obtained by transmission electron microscopy in a Jeol 200 keV. Magnetic properties were studied from the hysteresis loops at room temperature after saturating with a maximum field of 1 T in a PAR 4500 vibrating sample magnetometer. Saturation magnetization (Ms), squareness (Mr/Ms; Mr is the remanent magnetization), and coercive field (Hc) were obtained for sample M10 heated at 1200 and 1400°C.

RESULTS AND DISCUSSION

Samples M10, M20, and M30 consist of amorphous spherical particles with a broad size distribution, from 0.05 to 0.7 μm, similar to the samples previously obtained with a lower amount of Fe (15) (data not shown).

The evolution with temperature of the precursor particles was followed by thermal analysis and it is illustrated for sample M10 (Fig. 1). From the TG curve, the total weight loss when heated up to 1200°C was 30%. It can be observed that the maximum loss is taking place in the first stage of the heating process, between 20 and 300°C, which can be assigned to the elimination of methanol, adsorbed water, and impurities coming from the precursors. An exothermic peak is observed at around 222°C in the DTA curve, which can be

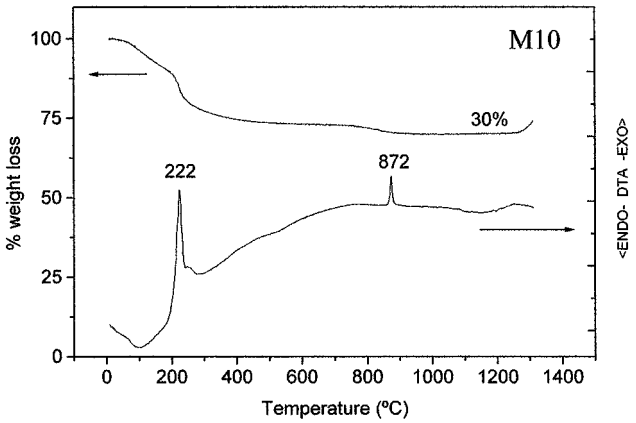

FIG. 1. Thermogravimetric and differential thermal analyses for sample M10.

assigned to the decomposition of the nitrate anions remaining in the sample. The exothermic peak at 872°C could be assigned to the crystallization of the pseudo-tetragonal mullite, which takes place at temperatures significantly lower than those reported for pure mullite, prepared by similar procedure (15). This behavior has been explained by the incorporation of iron to the mullite structure (15). It has been shown that the total incorporation of iron to the mullite structure and the transformation of pseudo-tetragonal–orthorhombic mullite take place at about 1200°C (15). Therefore, the precursor samples were heated at 1200°C, resulting in the formation of cristobalite (C), hema-

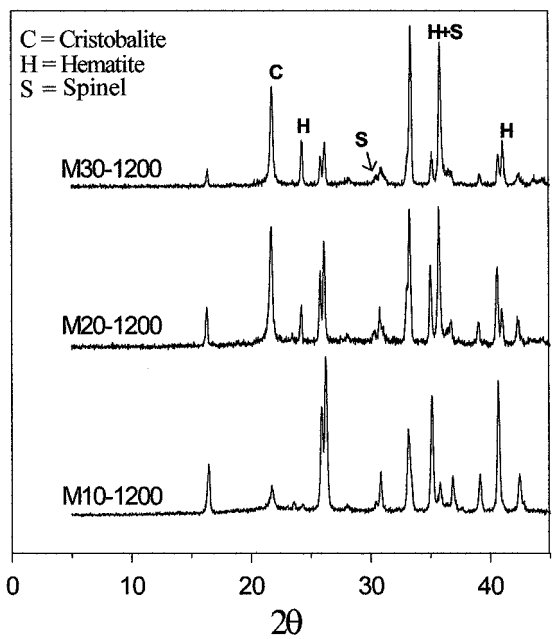

FIG. 2. X-ray diffraction patterns for Fe-doped mullite samples heated at 1200°C.

tite (H), and a spinel iron oxide (S) in addition to mullite (Fig. 2). The spinel iron oxide could be any term of the solid solution Fe_3O_4-γ-Fe_2O_3 with possible Al substitution. The precise nature of this spinel iron oxide phase is not a simple question due to the similar lattice parameters for these compounds and the small particle size that gives rise to the broadening of the X-ray peaks and therefore a significant uncertainty in the peak position (17). In relation to the mullite structure, the splitting of the peak at $2\theta \sim 26^\circ$, corresponding to the 120 and 210 reflections, suggests the formation of orthorhombic mullite (18). It is note worthy that cristobalite and hematite appear more clearly for the samples with a higher amount of Fe (sample M20, 1200°C and M30, 1200°C) while the spinel iron oxide remains invariable for all the samples. Moreover, when sample M10 was heated at higher temperatures (1400°C), the spinel peaks appeared more clearly defined in the diffractogram, whereas those of hematite dissapeared (Fig. 3), which may indicate the transformation of this iron oxide to the spinel phase. The diffractogram also shows the formation of a significant amount of cristobalite at this temperature (Fig. 3). This is as expected since the amount of Si and M^{3+} (M = Al + Fe) added in the initial solution are kept constant, and therefore, when the Fe solubility limit is overtaken, an excess of Si with respect to Al must result, which crystallizes into the cristobalite at high temperatures. From a magnetic point of view, sample M10 heated at 1400°C is the most interesting one since the iron containing phase present in the samples is a spinel in addition to mullite.

TEM pictures of samples M10-1200 and M10-1400 are shown in Fig. 4. Particles are hardly distinguishably in the sample heated at 1200°C. However, the formation of well-defined spherical particles with a diameter of around 13 ($\pm$ 4) nm inside the mullite matrix can be observed when the composite is heated at 1400°C (Fig. 4, Table 2). The formation of iron oxide particles has been previously observed in other matrices such as ferrisilicates of ZSM-5-type (19) and zircon (12). However, in the first case no magnetic phases were observed, whereas in the case of zircon a magnetic spinel was detected after heating at 900°C, which transforms in nonmagnetic hematite at 1200°C. In our case, the spinel particles in the mullite matrix do not transform even after heating at 1400°C. γ-Fe_2O_3 to α-Fe_2O_3 transformation has been reported to take place at temperatures between 370 and 600°C, depending on the origin of the sample and the presence of foreign ions such as Al, which retard the transformation (20, 21). But also the mechanism of transformation appears to depend on the crystal size. Ultrafine maghemite particles of 5 nm transform to hematite at around 500°C by a chain mechanism that involves recrystallization of up to 100 particles and formation of big hematite particles of around 40–70 nm (20). However, when these particles are dispersed in a silica matrix, the transformation is retarded to around 900°C (4), that is, when the matrix allows the particles to migrate and aggregate. It should be emphasized that a stable magnetic iron oxide

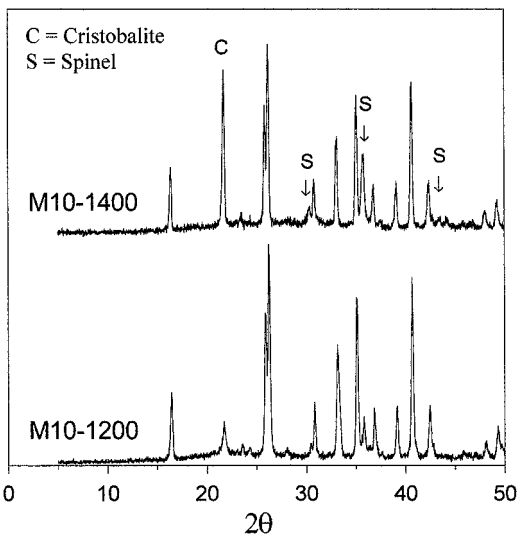

FIG. 3. X-ray diffraction patterns for sample M10 heated at 1200 and 1400°C.

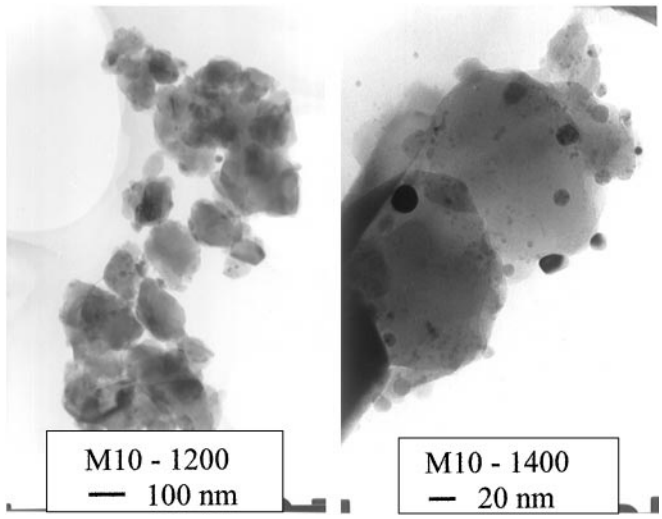

FIG. 4. TEM micrographs of sample M10 heated at 1200 and 1400°C.

TABLE 2
Particle Size and Magnetic Properties of Sample M10

Sample	Thermal treatment (°C)	γ-FeO_3 Particle size (TEM) (nm)	Magnetic properties		
			Hc (Oe)	Ms (emu/g)	Mr/Ms
M10-1200	1200	—	205	1,0	0.38
M10-1400	1400	13 $\pm$ 4	546	3,3	0.47

composite at a temperature as high as 1400°C has not been reported before. The mullite structure seems to be an ideal host matrix for keeping the magnetic nanoparticles apart and avoiding sintering and phase transformations, even after treatment at such a high temperature.

The magnetic behavior of samples M10-1200 and M10-1400 at room temperature is presented in Fig. 5. In both cases, the material shows hysteresis loops, in contrast to the iron-doped mullite below the iron solubility limit, which is expected to give rise to a typical paramagnetic behavior as is the case for other iron-doped ferrisilicates (19). Over the solubility limit, the iron ions are aggregated-forming particles with a magnetic order that are responsible for the hysteresis loops. The saturation magnetization values (Ms) after saturating with a field of 1 T are 1 and 3.3 emu per gram of composite for samples M10-1200 and M10-1400 respectively (Table 2). Considering that part of the iron ions is incorporated into the mullite structure ($\sim$ 12% Fe_2O_3), the fraction of iron involved in the formation of the nanosize particles is around 5.5 wt% Fe_2O_3. Thus, the magnetization values normalized to that iron excess are 18 and 60 emu/g for samples M10-1200 and M10-1400, respectively. The lowest Ms value observed for the sample after heating at 1200°C is due in part to the presence of hematite (Fig. 3), being on the same order of magnitude as that reported for disorder γ-Fe_2O_3 particles of around 5 nm in diameter (22). The highest Ms value is similar to the saturation magnetization for well-crystallized γ-Fe_2O_3 particles of around 10 nm (22), which is closer to the size of the magnetic particles observed by TEM in our composite after heating at 1400°C (Fig. 4). Therefore, the increase in Ms values with the heat treatment from samples M10-1200 to M10-1400 can be attributed not only to the hematite-to-spinel-iron-oxide transformation, which could take place as a consequence of the oxygen lost when heating above 1000°C (23), but also to the improvement in crystal order, which is rather evident from the TEM pictures (Fig. 4).

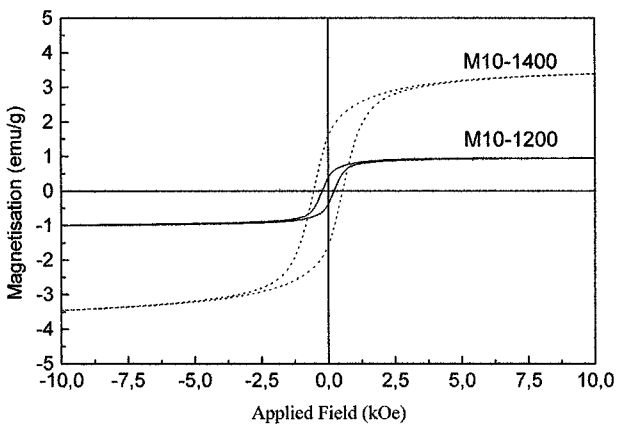

FIG. 5. Magnetization curves at room temperature for sample M10 heated at 1200 and 1400°C.

The coercivity values obtained for the iron oxide/mullite composite heated at 1200 and 1400°C are shown in Table 2. Coercivity increases strongly with the temperature treatment from 205 to 546 Oe. Additionally, the squarness value (Mr/Ms) after treatment at 1400°C is close to the theoretical value, 0.5 for single-domain noninteracting particles, suggesting that the magnetic particles are dispersed in the matrix as was observed by TEM (Fig. 4). However, neither γ-Fe_2O_3 particles between 10 and 5 nm in diameter or γ-Fe_2O_3/SiO_2 composites with particle sizes in this range showed any coercivity at room temperature or very low values (10 Oe) (6, 22). The origin of such a high coercivity in the iron oxide/mullite composites can be attributed to mainly three factors: shape anisotropy, magnetocrystalline anisotropy, and induced anisotropies. In our case, induced anisotropies, in particular stress-induced anisotropy, is the most probable and it would even explain the increase in coercivity from sample M10-1200 to sample M10-1400. This kind of anisotropy induced by interfacial stress has been suggested to enhance the coercivity of γ-Fe_2O_3 films deposited on Si substrate (24) as well as for γ-Fe_2O_3 spherical particles (0.1 μm in diameter) coated by a silica layer, the coercivity of which was increased from 200 up to 520 Oe (25).

CONCLUSIONS

A new magnetic nanocomposite that preserves its magnetic character after heating at 1400°C has been prepared by spray pyrolysis. The composite consists of nearly spherical particles of a spinel iron oxide of around 13 nm in diameter dispersed in a mullite matrix. The mullite has been shown to be an excellent matrix to keep the magnetic particles apart, avoiding sintering during the heat treatment and therefore making the γ-Fe_2O_3 to α-Fe_2O_3 transformation more difficult. Anisotropy induced by interfacial stress has been suggested to enhance the coercivity of this material, which has been found to be extraordinary high (around 500 Oe at room temperature) in comparison to the magnetic particle size.

ACKNOWLEDGMENTS

We thank Research Project PB98-0525 for financial support and M. Alonso-Sañudo thanks the HB97-033 Acciones Integradas Project.

REFERENCES

1. R. F. Ziolo, E. P. Giannelis, B. A. Weinstein, M. P. O'Horo, B. N. Ganguly, V. Mehrotra, M. W. Russell, and D. R. Huffman, *Science* **257,** 219 (1992).
2. D. L. Leislie-Pelecky and R. D. Rieke, *Chem. Mater.* **8,** 1770 (1996).
3. F. Bentivegna, M. Nyvit, J. Ferre, J. P. Jamet, A. Brun, S. Visnovsky, and R. Urban, *J. Appl. Phys.* **85,** 2270 (1999).
4. C. Chanéac, E. Tronc, and J. P. Jolivet, *J. Mater. Chem.* **6,** 1905 (1996).

5. G. Enneas, A. Musinu, G. Piccaluga, D. Zedda, D. Gatteschi, C. Sangregorio, J. L. Stanger, G. Concas, and G. Spano, *Chem. Mater*. **10,** 495 (1998).
6. F. del Monte, M. P. Morales, D. Levi, A. Fernandez, M. Ocaña, A. Roig, E. Molins, K. O'Grady, and C. J. Serna, *Langmuir* **13,** 3627 (1997).
7. M. Do Carmo Rangel and F. Galembeck, *J. Catal.* **145,** 364 (1994).
8. N. F. Borelli, D. L. Morse, and J. W. H. Schreurs, *J. Appl. Phys.* **54,** 3344 (1983).
9. S. Mann and J. P. Hannington, *J. Colloid Interface Sci.* **22,** 326 (1988).
10. B. H. Sohn and R. E. Cohen, *Chem. Mater*. **9,** 264 (1997).
11. L. Zhang, G. C. Papaefthymiou, and J. Y. Ying, *J. Appl. Phys.* **81,** 6892 (1997).
12. P. Tartaj, T. Gonzalez-Carreño, C. J. Serna, and M. Ocaña, *J. Solid State Chem.* **128,** 102 (1997).
13. C. Cannas, D. Gatteschi, A. Musinu, G. Piccaluga, and C. Sangregorio, *J. Phys. Chem. B* **102,** 7721 (1998).
14. H. Scheneider, *J. Am. Ceram. Soc*. **70,** C43 (1987).
15. M. Ocaña, A. Caballero, T. González-Carreño, and C. J. Serna, *Mater. Res. Bull.* **35,** 775 (2000).
16. K. Okada, N. Otsuka, and S. Somiya, *Ceram. Bull.* **70,** 1633 (1991).
17. M. P. Morales, S. Veintemillas, M. I. Montero, C. J. Serna, A. Roig, Ll. Casas, B. Martínez, and F. Sandiumenge, *Chem. Mater*. **11,** 3058 (1999).
18. ASTM file No. 15-776.
19. A. Lopez, F. J. Lázaro, J. L. García-Palacios, A. Larrea, Q. A. Pankhurst, C. Martínez, and A. Corma, *J. Mater. Res.* **12,** 1519 (1997).
20. R. M. Cornell and U. Schwertmann, *in* "The Iron Oxide," p. 363. VCH, Weinheim, Germany, 1996.
21. E. Wolska and U. Schwertmann, *Solid State Ionics* **32/33,** 214 (1989).
22. J. M. D. Coey, *Phys. Rev. Lett*. **27,** 1140 (1971).
23. A. Muan, *J. Am. Ceram. Soc*. **40,** 121 (1957).
24. W. D. Chang, T. S. Chin, H. S. Wu, S. W. Chou, and J. H. Jou, *J. Appl. Phys.* **77,** 1184 (1995).
25. M. P. Morales, M. J. Muñoz-Aguado, J. L. García-Palacios, F. J. Lázaro, and C. J. Serna, *J. Magn. Magn. Mater*. **183,** 232 (1998).